Journal of Biomedical Optics

SPIEDigitalLibrary.org/jbo

Optimization via specific fluorescence brightness of a receptor-targeted probe for optical imaging and positron emission tomography of sentinel lymph nodes

Zhengtao Qin
David J. Hall
Michael A. Liss
Carl K. Hoh
Christopher J. Kane
Anne M. Wallace
David R. Vera

SPIE

Optimization via specific fluorescence brightness of a receptor-targeted probe for optical imaging and positron emission tomography of sentinel lymph nodes

Zhengtao Qin,[a,b,c,d] David J. Hall,[b,c,d] Michael A. Liss,[b,e] Carl K. Hoh,[b,c,d] Christopher J. Kane,[b,e] Anne M. Wallace,[b,e] and David R. Vera[b,c,d,e]
[a]University of California, San Diego, Department of Chemistry, La Jolla, California 92093
[b]University of California, San Diego, Moores Cancer Center, La Jolla, California 92093
[c]University of California, San Diego, Department of Radiology, La Jolla, California 92093
[d]University of California, San Diego, In Vivo Cancer and Molecular Imaging Center, La Jolla, California 92093
[e]University of California, San Diego, Department of Surgery, La Jolla, California 92093

Abstract. The optical properties of a receptor-targeted probe designed for dual-modality mapping of the sentinel lymph node (SLN) was optimized. Specific fluorescence brightness was used as the design criterion, which was defined as the fluorescence brightness per mole of the contrast agent. Adjusting the molar ratio of the coupling reactants, IRDye 800CW-NHS-ester and tilmanocept, enabled us to control the number of fluorescent molecules attached to each tilmanocept, which was quantified by ^{1}H nuclear magnetic resonance spectroscopy. Quantum yields and molar absorptivities were measured for unconjugated IRDye 800CW and IRDye 800CW-tilmanocept (800CW-tilmanocept) preparations at 0.7, 1.5, 2.3, 2.9, and 3.8 dyes per tilmanocept. Specific fluorescence brightness was calculated by multiplication of the quantum yield by the molar absorptivity and the number of dyes per tilmanocept. It predicted that the preparation with 2.3 dyes per tilmanocept would exhibit the brightest signal, which was confirmed by fluorescence intensity measurements using three optical imaging systems. When radiolabeled with ^{68}Ga and injected into the footpads of mice, the probe identified SLNs by both fluorescence and positron emission tomography (PET) while maintaining high percent extraction by the SLN. These studies demonstrated the feasibility of 800CW-tilmanocept for multimodal SLN mapping via fluorescence and PET–computed tomography imaging. *© The Authors. Published by SPIE under a Creative Commons Attribution 3.0 Unported License. Distribution or reproduction of this work in whole or in part requires full attribution of the original publication, including its DOI.* [DOI: 10.1117/1.JBO.18.10.101315]

Keywords: sentinel lymph node; specific fluorescence brightness; fluorescence imaging; positron emission tomography imaging; multimodality, IRDye 800CW, 800CW-tilmanocept, tilmanocept.

Paper 130221SSR received Apr. 8, 2013; revised manuscript received Jun. 5, 2013; accepted for publication Jun. 27, 2013; published online Aug. 19, 2013.

1 Introduction

A sentinel lymph node (SLN) is defined[1] as the first lymph node that receives lymph from a tumor. Consequently, the SLN is the first tissue to trap malignant cells that have metastasized from the primary cancer. To exploit this biological phenomenon, surgeons localize the SLN using a vital blue dye,[2] a radiopharmaceutical,[3] or both.[4] If, after a thorough pathologic examination, the SLN is free of tumor cells, the surgeon can conclude that the cancer has not spread. If the patient is a woman with breast cancer, the surgeon will reduce the extent of the surgery by not excising the remaining lymph nodes.[5] If the SLN is draining a melanoma, an SLN that is free of tumor cells is predictive of a better prognosis.[6]

Technetium-99m-labeled tilmanocept,[7] also known as [^{99m}Tc]-diethylenetriaminepentaacetic acid (DTPA)-mannosyl-dextran,[8] is a receptor-targeted radiopharmaceutical designed for SLN detection. Using an "instant kit" formulation[9] with the tradename *Lymphoseek*, a series of phase 1,[10,11] phase 2,[12] and phase 3[13,14] clinical trials, using intradermal, subareolar, and periturmoral administrations, demonstrated rapid SLN accumulation, high SLN retention, high concordance with vital blue dye, and no adverse events related to the radiopharmaceutical. Technetium-99m-labeled tilmanocept was approved for clinical use by the U.S. Food and Drug Administration in March 2013.[15]

Recent clinical trials[16,17] using a mixture of indocyanine green (ICG),[18] a low-molecular weight fluorescent dye that emits a near-infrared (NIR) photon, and *Nanocoll*,[19,20] a ^{99m}Tc-labeled microaggregate of albumin, have demonstrated the potential of SLN detection based on multimodal imaging. Assuming high affinity of ICG for albumin, the patient is first imaged with a single photon emission computed tomography, which is usually attenuation-corrected based on a computed tomography (CT) image. Guided by these preoperative images, the surgeon intraoperatively detects the SLNs using endoscopic imaging of the ICG fluorescence.

We recently proposed[9] multimodal SLN detection based on imaging with positron emission tomography (PET) with CT-based attenuation correction. PET provides higher spatial resolution, increased sensitivity, more accurate attenuation correction, and better scatter correction. After radiolabeling tilmanocept with ^{68}Ga, a generator-produced positron-emitting radionuclide, canine pelvic SLNs were imaged 1 h after a transrectal injection into the prostate gland.[21] Covalent attachment of Cy7, a cyanine fluorescent dye, to tilmanocept resulted in an

Address all correspondence to: David R. Vera, University of California, San Diego, Moores Cancer Center, 3855 Health Sciences Drive, La Jolla, California 92093. Tel: 858.822.2574; Fax: 858.246.0594; E-mail: dvera@ucsd.edu

NIR fluorescent-tagged tilmanocept,[22,23] which retained the properties exhibited by tilmanocept without the fluorescent tag. Fluorescent-labeled tilmanocept exhibited sub-nanomolar receptor affinity ($K_D < 1$ nM) to a macrophage cell line that expresses the receptor (CD206), as well as *in vivo* behavior consistent with SLN receptor-mediated accumulation.

Here we introduce a series of new dextran conjugates with different dye densities. The dyes are covalently conjugated to the dextran backbone. And the average number of dyes per dextran was measured via nuclear magnetic resonance (NMR). The specific fluorescence brightness was evaluated for the selection of the best imaging probe. Finally, ^{68}Ga was labeled to the fluorescent-tilmanocept and the feasibility of SLN PET and fluorescence imaging in a mouse model was demonstrated. To the best of our knowledge, this is the first example of dual-modality SLN-targeted nonparticulate imaging with ^{68}Ga and an NIR dye, IRDye 800CW.

2 Methods

2.1 *Synthesis: Conjugation of IRDye 800CW to Tilmanocept*

Conjugation of the optical reporter, a cyanine dye, to tilmanocept proceeded in a manner previously described.[24] The NIR dye was covalently coupled to the amino-terminated leashes on the dextran backbone of DTPA-mannosyl-dextran (tilmanocept, Navidea Biopharmaceuticals, Ohio). The mean number of DTPA, mannose, and amines per dextran of the tilmanocept preparation was 4.4, 16.8, and 5.5, respectively. The mean molecular weight was 16,738 g/mol and Stokes radius was 7.7 nm. Conjugates with different IRDye 800CW to tilmanocept ratios were prepared. Briefly, tilmanocept (0.25 μmol) was combined with varying amounts (molar excess of 1 to 10 equivalents) of IRDye 800CW-NHS-ester (LI-COR Biosciences, Nebraska) in 1.1 ml dimethyl sulfoxide. After brief vortexing, the mixture was incubated overnight on a rolling rotor at 30°C. After diluting the reaction mixture with deionized water, IRDye 800CW-tilmanocept (800CW-tilmanocept) was purified by centrifuging the product through an ultrafiltration system (Ultra 15, Amicon Corp., Maryland, 3 kDa molecular weight cut-off). After five times of centrifugation, deionized water was added to the concentrated retentate and a sample was removed for analysis of purity. The centrifugation was repeated until no free IRDye 800CW could be detected in the retentate as measured by high-performance liquid chromatography (HPLC) with fluorescence detection. The product was lyophilized, weighed, and redissolved in phosphate-buffered saline (PBS) to form a stock solution with a final concentration of 1.0×10^{-4} M. Purity of the final product was confirmed by size exclusion (TSKgel G2000SWxl, Tosoh Bioscience LLC, Tokyo, Japan) HPLC (System Gold, Beckman-Coulter, California) using 0.9% saline as the mobile phase. The eluate was monitored by UV absorbance and fluorescence (L-7480, Hitachi America, Ltd., Michigan).

2.2 *Quantification of Fluorophore Density*

NMR spectroscopy was performed to measure the average number of conjugated IRDye 800CW molecules attached to each tilmanocept molecule. Purified 800CW-tilmanocept was dissolved in D_2O to form a concentrated solution. The sample was analyzed on a 500 MHz NMR spectrometer (ECA 500, JEOL Corp, Ohio). The fluorophore density R, the average number of dyes per dextran backbone, was calculated using Eq. (1):

$$R = \frac{\frac{A_{Ha}}{8}}{A_{Hb}} \times 62, \tag{1}$$

where A_{Ha} equals the area under the peak designated H_a at 7.7 ppm and A_{Hb} equals the area under the two peaks designated H_b at 4.8 and 5.2 ppm.

2.3 *Statistical Analysis of IRDye 800CW Density Distribution*

We employed a statistical model to predict the distribution of IRDye 800CW attached to each tilmanocept. The model was previously used to predict the distribution of iodine atoms after radiolabeling of proteins[25] and was later applied by Meares and Goodwin[26] to study the distribution of chelators after covalent attachment to antibody molecules. The quantity

$$fS_n = \frac{m!n}{n!(m-n)!R}(R/m)^n(1-R/m)^{m-n} \tag{2}$$

represents the theoretical fraction of 800CW-tilmanocept molecules with n IRDye 800CW molecules covalently coupled to the amino-terminated leashes of the dextran backbone. The quantity m is the maximum number of amino-terminated leashes in the tilmanocept molecule; we set m equal to 6 based on the average number of free amino groups in the tilmanocept preparation. The average number of IRDye 800CW molecules per tilmanocept (IRDye 800CW density) is represented by the variable R. We calculated fS_n values for 800CW-tilmanocept preparation having average 800CW densities of 0.25, 0.5, 1.0, 2.0, and 3.0 mol/mol. Equation (2) assumes that the IRDye 800CW-NHS-ester reacts with all of the amino-terminated leashes with equal probability and that attachment to an amino group renders the reaction site unreactive and does not alter the probability of a reaction to the remaining sites. Using conservation of mass, the fraction of tilmanocept molecules without any attached dye (fuS) can be calculated as

$$fuS = 1 - R\sum_{n}^{m}\frac{fS_n}{n}. \tag{3}$$

2.4 *Characterization of Optical Properties*

Absorption spectra (Varian Carey 3E, Agilent Technologies, CA) were obtained between 650 and 850 nm (1 nm slit width, 1 nm step size) for both IRDye 800CW-NHS-ester and five 800CW-tilmanocept conjugates with a different dye density each. Samples were dissolved in PBS followed by brief shaking. The solutions were diluted with PBS to five concentrations and measured in a cuvette with a 10 mm path length. Emission spectra (Fluorolog 3, Horiba Jobin Yvon Inc., New Jersey) were obtained for each 800CW-tilmanocept conjugate and unconjugated IRDye 800CW-NHS-ester. Samples were excited at 758, 780, and 805 nm, respectively, and emission spectra (750 to 850 nm, 5 nm slit width) were acquired.

The molar absorptivities (ε) of unconjugated IRDye 800CW and 800CW-tilmanocept conjugates were calculated in the following manner. Absorption at 758, 780, or 805 nm was measured for each sample at five different dilutions. All absorbance values were below 0.05. When the absorbance was plotted as a function of the IRDye 800CW concentrations, ε equaled the gradient of the regression line. The standard errors for ε were generated from the linear regression.

Quantum yields (Φ) for free IRDye 800CW-NHS-ester and 800CW-tilmanocept were calculated in the following manner. Applying a similar method outlined by Williams et al.,[27] the integral of the corrected fluorescence spectrum over 760 to 850 nm of each sample dilution was plotted against the absorbance at the individual excitation wavelength. The gradient yielded the relative quantum yield of each sample. The standard errors for Φ were generated from the linear regression. The absolute value of the quantum yield and standard error for unconjugated IRDye 800CW were obtained from three measurements on an integrating sphere Quanta-phi (HORIBA Scientific, New Jersey). The relative quantum yield values for each of the 800CW-tilmanocept conjugates were scaled to the absolute values by multiplying the ratios of the relative quantum yield of each 800CW-tilmanocept to IRDye 800CW, and the absolute quantum yield of the IRDye 800CW.

We calculated fluorescent brightness per molecule of IRDye 800CW and per molecule of 800CW-tilmanocept. The brightness per molecule of IRDye 800CW was calculated as the product of molar absorptivity (ε) and the quantum yield (Φ). The multiplication of R and $\varepsilon\Phi$ yielded the specific fluorescence brightness $\varepsilon\Phi R$, which provided a measure for the contrast agent. This parameter was used as the design criterion for optimization of our fluorescent probe. The relative errors for the brightness values were generated as the quadratic sum[28] of the relative errors of ε and Φ. The standard deviation of dye density R from three NMR measurements was <0.3% of the absolute value. It was neglected in calculations of the errors for the specific fluorescence brightness.

In vitro fluorescence intensity measurements of five 800CW-tilmanocept conjugates were performed on three different fluorescence imaging systems. Each imager represents a different experimental setting and uses a different set of excitation and emission wavelengths. The Optix MX (Advanced Research Technologies Inc., Montreal, Canada) uses an excitation wavelength of 758 nm and an emission filter set consisting of a 780 nm long-pass filter and a 782 nm bandpass filter with a 20 nm bandwidth. The Fluobeam 800 (Fluoptics, Grenoble, France) excites with a wavelength of 780 nm and employs a long-pass emission filter at 800 nm. The da Vinci SI surgical system (Intuitive Surgical Inc., California) uses an excitation laser of 805 nm and applies a long-pass emission filter at 830 nm. Solutions (640 μL) in eppendorf centrifuge tubes with the same concentration of 800CW-tilmanocept (781 nM) were placed under the cameras within the field-of-view. The same volume of PBS was used as a blank control. All samples were arranged in a manner to ensure uniform illumination. Images were acquired and a region of interest (ROI) was drawn within each sample to calculate the fluorescence signals; an ROI over the PBS represented the background noise. The signal-to-noise ratio (SNR) was calculated by dividing the signal from the ROI with the background noise. The maximum fluorescence intensity within each ROI was obtained using Optiview (Advanced Research Technologies Inc.) and ImageJ software (National Institutes of Health, Bethesda).

For each of the three excitation wavelengths, the brightness and the ROI fluorescence intensity measurements of all 800CW-tilmanocept conjugates with different IRDye 800CW densities were compared. The molar brightness and ROI fluorescence intensity were normalized through dividing each measurement within a given wavelength by the highest value, which was provided by the $R = 2.3$ mol/mol conjugate for all three wavelengths.

2.5 *Radiolabeling and Radiochemical Purity*

Radiolabeling of 800CW-tilmanocept with ^{68}Gawas performed using a previously described method.[21] Briefly, a ^{68}Ga generator (IGG100, Eckert & Ziegler Isotope Products, Berlin, Germany) was eluted with 5 ml 0.1 N HCl. A volume (30 μL) containing 3 nmol of 800CW-tilmanocept was combined in a polypropylene vial with 50 μL of 2.0 M sodium acetate solution and 0.5 mL of the generator elute. The reaction mixture was allowed to stand at room temperature for 15 min. Finally, 0.5 mL PBS (pH 7.2, 0.1 mol/L phosphate and 0.15 mol/L chloride) was added to the reaction mixture to adjust the pH value to 7. Doses (40 μL) were drawn into insulin syringes with 28 gauge needles. Instant thin layer chromatography (ITLC) using Whatman-31ET (Whatman Ltd., Michigan) as the stationary phase and acetone as the mobile phase was performed using standard technique to measure the radiochemical purity. The radiolabeled product was characterized by HPLC using UV absorbance, fluorescence, and radioactivity detection (Model 170, Beckman-Coulter).

2.6 *Fluorescent Purity*

Purity of fluorescent label was measured by scanning the ^{68}Ga-labeled 800CW-tilmanocept ITLC strips developed in CH_3OH/H_2O (85/15, v/v) with the Optix MX fluorescence imaging system ($\lambda_{ex} = 758$ nm, $\lambda_{em} = 780$ to 792 nm). An ITLC of free IRDye 800CW was also performed and scanned on the Optix MX. This sample was prepared by combining 100 nmol IRDye 800CW-NHS-ester in 1 mL PBS. After standing for at least 30 min at room temperature, a drop of the solution was applied to a silica gel ITLC strip (green label, Biodex Medical Systems, New York) and developed with CH_3OH/H_2O (85/15, v/v).

2.7 *In Vivo Sentinel Lymph Node Fluorescence Imaging*

In vivo SLN mapping was performed using a healthy mouse model. After subcutaneous footpad injections, optical properties and the radioactivity profile of each popliteal lymph node was studied. Female Swiss Webster mice (18 to 24 g, five weeks old) were purchased from Charles River Labs. The *in vivo* procedures in this study were performed under a protocol approved by the Institutional Animal Care and Use Committee at University of California, San Diego.

Three mice were imaged for each 800CW-tilmanocept conjugate with fluorophore densities of 0.7, 1.5, 2.3, 2.9, and 3.8. All mice were anesthetized by inhalation of 1 to 2% isoflurane during the study. After induction of anesthesia, the lower abdomen and both legs of each mouse were shaved and 40 μL ^{68}Ga-labeled 800CW-tilmanocept (0.11 nmol) was

injected subcutaneously into one hind side of the footpad. Immediately after the injection, the footpad was massaged for 10 s. The mice were transferred to the imaging stage of the Optix MX for *in vivo* imaging, at 25 min postinjection. The footpad bearing the injection was taped onto the stage to avoid motion artifacts. The laser excitation and emission wavelengths were adjusted to the same values ($\lambda_{ex} = 758$ nm, $\lambda_{em} =$ 780 to 792 nm) as used to image the *in vitro* fluorescence intensity. An ROI was selected over the footpad and the SLN with a 1.5×1.5 mm^2 pixel size. The mice were euthanized 30 min postinjection. The popliteal and inguinal lymph nodes were excised. Images were viewed and analyzed with standard software (OptiView).

2.8 *PET Imaging*

Nuclear imaging was performed on a small-animal PET scanner (eXplore Vista DR, GE Healthcare, Wisconsin). Injections of ^{68}Ga-labeled 800CW-tilmanocept (~0.11 nmol) were performed in mice as stated in Sec. 2.6. The syringes containing radioactivity were assayed in a dose calibrator CRC-15W (Capintec Inc., New Jersey) before and after injection for the accurate determination of the injected dose. Mice were placed on the stage in a supine position. PET acquisitions were conducted in list mode for a 25-min dynamic scan (400 to 700 keV energy window). Cross-sectional images were reconstructed into five 5-min frames. SNR was defined as dividing the radioactivity counts per pixel from the SLN by the radioactivity counts per pixel from the background outside of the animal.

2.9 *Nuclear Counting and SLN IRDye 800CW Calculation*

The excised lymph nodes were assayed for radioactivity using a 400 to 600 keV window (Gamma 9000, Beckman Instruments, California) and compared to a counting standard of a known dilution of the injectate. The percent of injected dose (%ID) of tilmanocept was calculated by comparison of the tissue counts with counts from the counting standard. Calculation of the amount of 800CW-tilmanocept within each SLN was based on the %ID of tilmanocept. The amount of IRDye 800CW within each SLN was calculated based on the amount of 800CW-tilmanocept and the IRDye 800CW density. The percent SLN extraction[23] was calculated as the difference between the SLN and distal lymph node counts divided by the sum of the SLN and distal lymph node counts.

3 Results

3.1 *Synthesis*

The chemical structure of ^{68}Ga-labeled 800CW-tilmanocept is illustrated in Fig. 1(a). The receptor-binding multimodal imaging probe is composed of *NC* units of amino-terminated leashes, *ND* units of DTPA, which chelate the nuclear imaging reporter

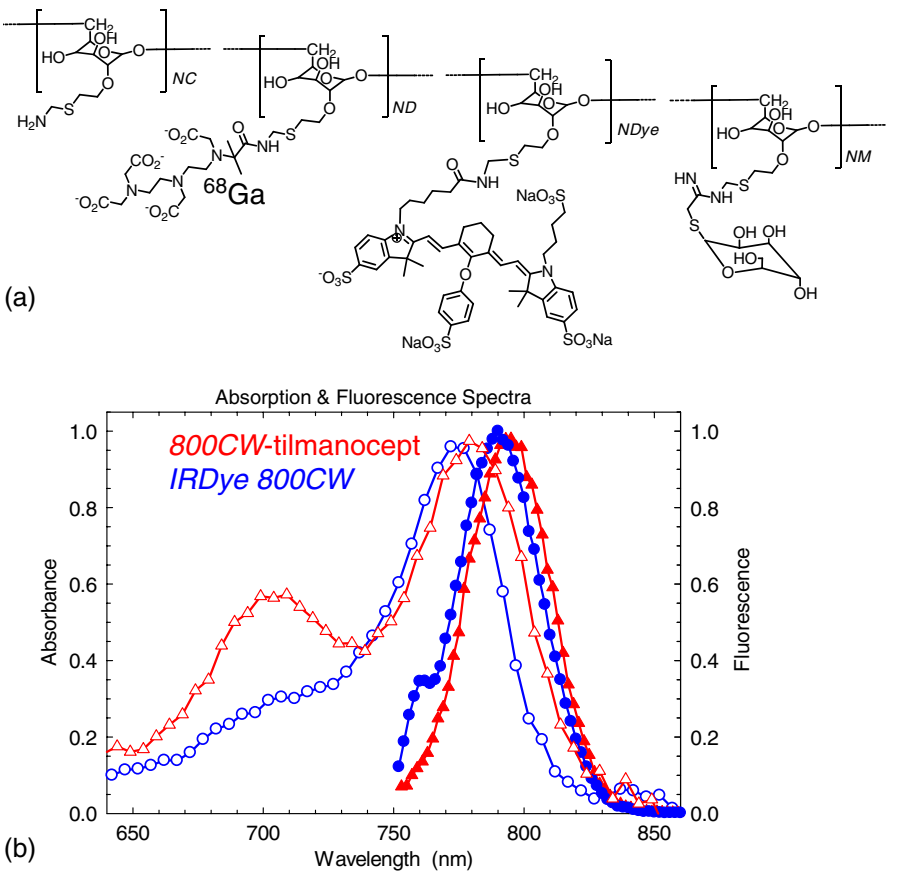

Fig. 1 Chemical structure of ^{68}Ga-labeled 800CW-tilmanocept and its normalized absorbance (open) and fluorescence (solid) spectra. (a) The receptor-binding multimodal imaging probe is composed of *NC* units of amino-terminated leashes, *ND* units of diethylenetriaminepentaacetic acid (DTPA) groups, which chelate the nuclear imaging reporter ^{68}Ga, *NDye* units of the optical imaging reporter IRDye 800CW, and *NM* units of mannose, the receptor substrate. (b) Attachment of IRDye 800CW to tilmanocept produces a 6 nm red shift and an increase in the nonradiative peak (800CW-tilmanocept: triangle; IRDye 800CW: circle).

^{68}Ga, *NDye* units of the optical imaging reporter IRDye 800CW, and *NM* units of mannose, the receptor substrate. Figure 1(b) is the normalized absorbance and fluorescence spectra of free IRDye 800CW and an 800CW-tilmanocept preparation having a mean fluorophore density of 2.3 dyes per tilmanocept. The spectra demonstrated absorption and emission peaks of the conjugated product with a 6 nm visible red shift, compared to the unconjugated IRDye 800CW. A similar phenomenon was observed for Cy7-tilmanocept.[23]

The HPLC chromatograms of unconjugated IRDye 800CW molecule exhibited absorbance and fluorescence peaks with an elution volume of 28 mL. All conjugates exhibit absorbance and fluorescence peaks at an elution volume of 10 mL with no detectable peaks at 28 mL.

3.2 *Calculation of Fluorophore Density*

Figure 2 is a portion (4 to 8 ppm) of a proton NMR spectrum for 800CW-tilmanocept ($R = 3.8$) in D_2O. H_a represents 8 protons on IRDye 800CW molecules; H_b describes protons on α_1 carbon of dextran backbone. There are three benzene rings on each IRDye 800CW molecule and six protons at the ortho- positions to the sulfonate, which are heavily deshielded due to the magnetic anisotropy of the ring. Two allylic protons close to the cyclohexenyl ring also have a far downfield chemical shift, as a result of the ring current from the phenoxy group. Thus, chemical shifts of those eight protons are at 7.7 ppm. The dextran backbone of tilmanocept is composed of 62 glucose molecules with α-1, 6 glycosidic linkages, with certain portion of branches by α-1, 3 glycosidic linkages. Two neighboring oxygen atoms are in short range, resulting in deshielding effect toward the adjacent protons. As a result, the protons on the anomeric α_1 carbons have two unique chemical shifts at around 4.8 and 5.2 ppm.

The fluorophore density could be controlled by the molar ratio of the coupling reactants, IRDye 800CW-NHS-ester and tilmanocept. Figure 3 demonstrates this ability, where the reactant ratios from 1 to 10 mole of IRDye 800CW-NHS-ester per

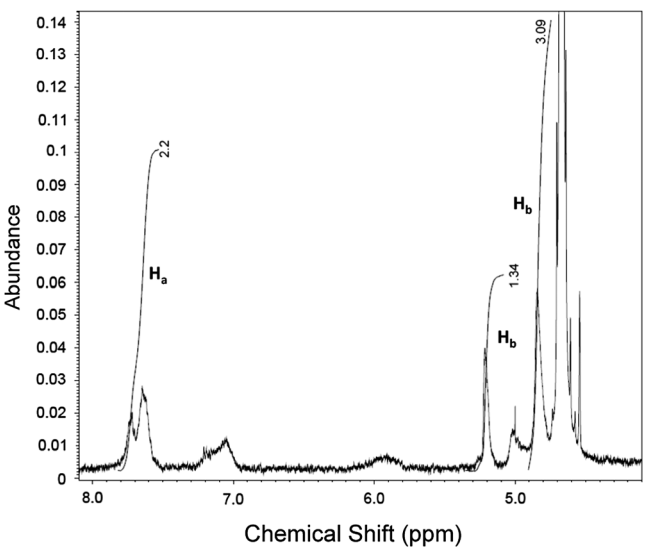

Fig. 2 Proton NMR spectrum (4 to 8 ppm) for 800CW-tilmanocept in D_2O. H_a represents eight protons on IRDye 800CW; H_b represents protons on α_1 carbon of the dextran backbone. This spectrum was acquired from a conjugate with an average of 3.8 IRDye 800CW molecules per tilmanocept.

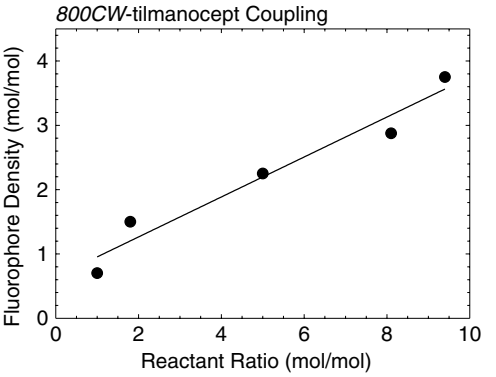

Fig. 3 The average number of IRDye 800CW molecules per tilmanocept can be controlled during the chemical synthesis by adjusting the molar ratio of the IRDye 800CW-NHS-ester to tilmanocept.

mole of tilmanocept produced 800CW densities from 0.7 to 3.8 per tilmanocept. Five IRDye 800CW densities were prepared: 0.7, 1.5, 2.3, 2.9, and 3.8 mol/mol.

3.3 *Statistical Analysis of IRDye 800CW Density Distribution*

Table 1 lists the percentage of 800CW-tilmanocept molecules composed of n IRDye 800CW molecules for preparations with an average R of 0.25, 0.50, 1.0, 2.0, and 3.0 800CWs per tilmanocept. Attachment of IRDye 800CW molecules to the tilmanocept macromolecule will result in a distribution of conjugates bearing different numbers of IRDye 800CW molecules per tilmanocept. For example, when a preparation contains a ratio of 0.25 IRDye 800CW molecules to one tilmanocept molecule, Eq. (2) predicts that 80% of the 800CW-tilmanocept molecules will exist as conjugates with a single IRDye 800CW attachment and that 18% of the 800CW-tilmanocept molecules will have two IRDye 800CW molecules attached to tilmanocept. When the average number of IRDye 800CW molecules per tilmanocept is 1.0, Eq. (2) predicts that an equal percentage (40%) of 800CW-tilmanocept molecules will consist of single and double substitutions.

3.4 *Characterization of Optical Properties*

Covalent attachment of IRDye 800CW to tilmanocept altered the absorbance spectra. Figure 4 is the absorbance spectra (dye concentrations of 150 nM) of unattached IRDye 800CW and 800CW-tilmanocept conjugates of different IRDye 800CW densities. The absorbance profile of 800CW-tilmanocept was significantly influenced by the fluorophore density. The ratio of nonradiative overtone hump at 710 nm (confirmed by comparison of excitation and absorption scans) to the peak at 780 nm increased when more dyes were attached. At same dye concentration, the conjugate with a mean density of 2.3 dyes per tilmanocept (green, hexagon) had the highest absorbance at 780 nm, while the conjugate with 0.7 dyes per tilmanocept (cyan, triangle) had the lowest absorbance. The conjugates with 1.5 (red, circle), 2.9 (blue, diamond), and 3.8 (pink, square) dyes per tilmanocept had intermediate absorbance values at 780 nm. All conjugates exhibited less absorbance at this wavelength compared to free fluorophore (black).

The optical characteristics of the conjugates with different IRDye 800CW densities were determined at three excitation

Table 1 Percentage of 800CW-tilmanocept molecules composed of *n* IRDye 800CW molecules.

Number of IRDye 800CW molecules attached per tilmanocept	$fS_n \times 100$ (%)				
	R, average IRDye 800CW molecules per tilmanocept (mol/mol)				
n	0.25	0.50	1.0	2.0	3.0
1	0[a]	65	40	13	3.1
2	18	29	40	33	16
3	1.5	5.4	16	33	31
4	0.66	0.49	3.2	16	31
5	0.015	0.022	3.2	4.1	16
6	0.00013	0.00040	0.013	0.41	3.2
Percent of tilmanocept with IRDye 800CW	22.6[b]	40.7	66.5	91.2	98.4

Note: The number of available attachment sites (*m*) equals 6.
[a]See Eq. (2).
[b]See Eq. (3).

wavelengths. The molar absorptivity ε decreased dramatically after the attachment to tilmanocept at low fluorophore density ($R = 0.7$). With increasing fluorophore density, the absorptivity per mole of fluorophore increased to a peak value at 2.3 and then decreased [Fig. 5(a)]. The relative error of the molar absorptivity and quantum yield measurements were <9 and 11%, respectively. The brightness and quantum yield per attached fluorophore were lower than the free fluorophore. For free IRDye 800CW, the molar absorptivity ε and quantum yield Φ in PBS at 780 nm were measured to be 122,980± 19,382 $M^{-1} \cdot cm^{-1}$ and 0.12 ± 0.0002, respectively. The quantum yield decreased with increasing fluorophore density [Fig. 5 (b)]. As a result of the changing molar absorptivity and quantum yield, the IRDye 800CW brightness $\varepsilon\Phi$ [Fig. 5(c)] and the specific fluorescence brightness $\varepsilon\Phi R$ [Fig. 5(d)] exhibited peak values at fluorophore density of $R = 2.3$. At an excitation wavelength of 780 nm, the calculated specific fluorescence brightness for 2.3 800CW-tilmanocept conjugate was ~4.7 times higher than the 0.7 conjugate. The 800CW-tilmanocept brightness values at 780 nm were higher than 758 nm, and the lowest values were at 805 nm.

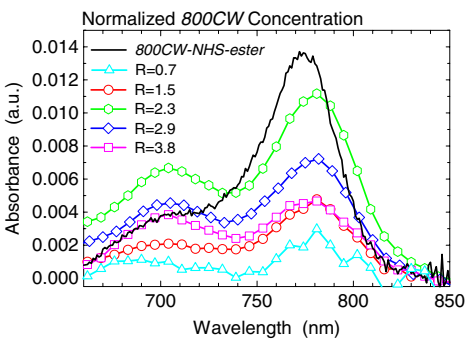

Fig. 4 Absorbance spectra (normalized to equal an IRDye 800CW concentration of 150 nM) of unattached IRDye 800CW and 800CW-tilmanocept conjugates with different IRDye 800CW densities: (black) IRDye 800CW-NHS-ester, (cyan, triangle) 0.7 dyes per tilmanocept, (red, circle) 1.5 dyes per tilmanocept, (green, hexagon) 2.3 dyes per tilmanocept, (blue, diamond) 2.9 dyes per tilmanocept, (pink, square) 3.8 dyes per tilmanocept.

In vitro fluorescence images confirmed our specific fluorescence brightness calculations. Normalized 800CW-tilmanocept brightness when plotted against the IRDye 800CW density matched the normalized ROI intensities [Fig. 6(a), 6(c), and 6(e)]. Both parameters peaked at fluorophore density of $R = 2.3$ for each of the three excitation wavelengths. The ROI intensity for the conjugate with fluorophore density of $R = 0.7$ was the lowest. The ROI intensity of 800CW-tilmanocept with a density of $R = 2.3$ was much stronger, by a factor of 3.5 for excitation at 758 nm, 5.0 for excitation at 780 nm, and 6.4 for excitation at 805 nm. Figure 6(b), 6(d), and 6(e) shows images from the Optix MX, Fluobeam 800, and Firefly endoscopic camera of the da Vinci SI robotic surgical system. The conjugate with the fluorophore density of 2.3 provided the highest fluorescent intensity in each of the three images, which exhibited SNR values of 809:1 for the Optix MX, 90:1 for the Fluobeam 800, and 2.5:1 for the da Vinci SI robotic surgical system.

3.5 *Radiolabeling and Radiochemical Purity*

The radiolabeling yield and purity for the ^{68}Ga-labeled products were in excess of 98%. HPLC and ITLC demonstrated high radiochemical purity. The absorbance [Fig. 7(a)], fluorescence [Fig. 7(b)], and radioactivity [Fig. 7(c)] HPLC chromatograms

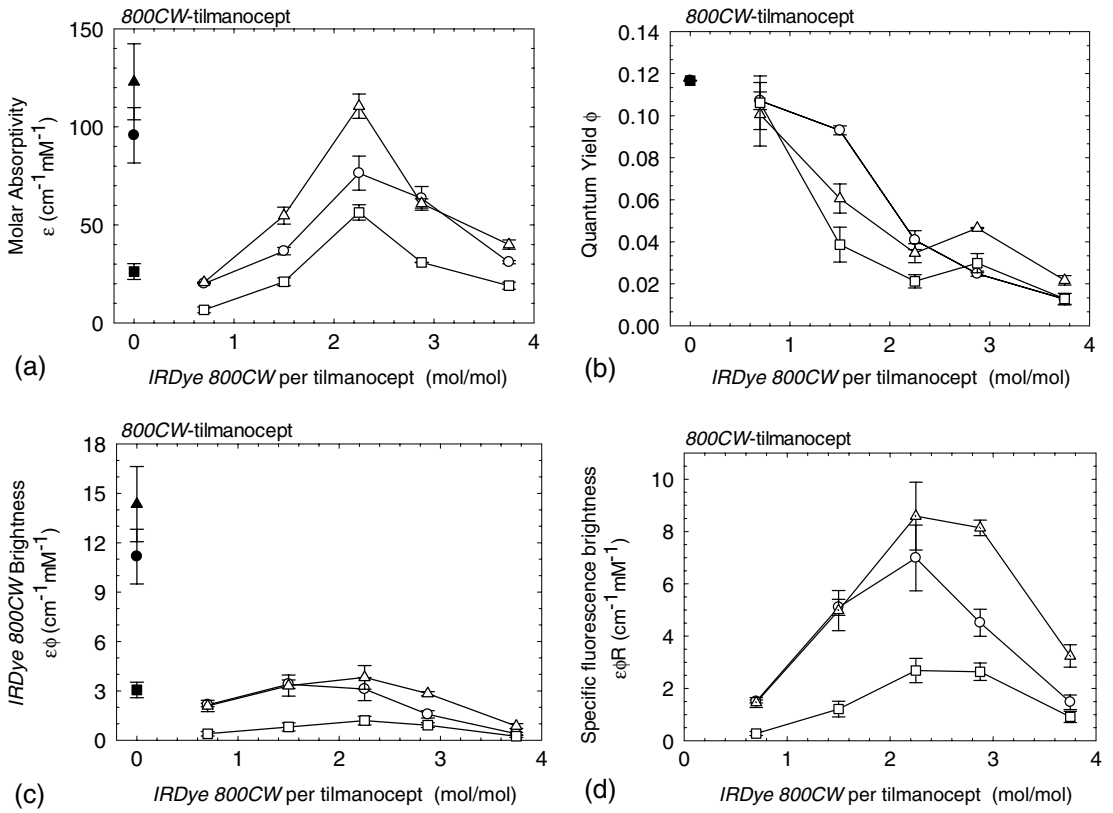

Fig. 5 Optical properties of five IRDye 800CW-tilmanocept (open symbols) conjugates at (circles) 758 nm, (triangles) 780 nm, and (squares) 805 nm. (a) Molar absorptivity ε (per mole of fluorophore). (b) Quantum yield Φ. (c) Brightness of IRDye 800CW $\varepsilon\Phi$. (d) Specific fluorescence brightness of 800CW-tilmanocept conjugate $\varepsilon\Phi R$ (per mole of tilmanocept). The solid symbols represent unattached IRDye 800CW.

exhibited a single component at the same elution volume. Radioactivity remained at the origin of the ITLC chromatograms [Fig. 7(d)], indicating high radiochemical purity for all ^{68}Ga-labeled 800CW-tilmanocept preparations. Gallium-68 DTPA compound, a possible impurity, travels to the solvent front.

3.6 *Fluorescent Purity*

The fluorescent purity of all preparations was in excess of 98%. Fluorescence scans of the ITLCs of ^{68}Ga-labeled 800CW-tilmanocept demonstrated high purity of the conjugate with fluorescent tag. More than 98% of the fluorescence and radioactivity remained at the origin [Fig. 8(a) and 8(c)]. Unconjugated IRDye 800CW traveled to the solvent front [Fig. 8(b) and 8(d)].

3.7 *In Vivo Sentinel Lymph Node Fluorescence Imaging*

Popliteal SLNs were identified by their fluorescence intensity after footpad injection. No detectable signals were observed from distal lymph nodes. For all mice, the percentage extraction of popliteal nodes exceeded 99%, which was consistent with our previous observations with ^{99m}Tc-labeled tilmanocept[8] and ^{99m}Tc-labeled Cy7-tilmanocept.[23] Among the five preparations, the $R = 2.3$ conjugate provided dramatically brighter signals than all other conjugates. *In vivo* imaging (Fig. 9) of the $R = 2.3$ 800CW-tilmanocept conjugate showed a bright popliteal node close to the injection site in the left hind leg. The color map is logarithmic with a peak value of 56 kilocounts. Based on the *ex vivo* nuclear counting, ~1.1 pmol of 800CW-tilmanocept molecules accumulated in the popliteal SLN. Consequently, the fluorescence signal with a peak intensity of 1.2 kilocounts in the SLN was originated from the 2.5 pmol of conjugated IRDye 800CW molecules. The right hind leg of the animal was scanned as a control, where no counts were observed above the background signal. When the same amount of 800CW-tilmanocept with dye density of $R = 0.7$ was administrated to the mice, a similar amount of the conjugate was trapped in the popliteal node; however, the node was not identifiable against the background signal (image not shown).

3.8 *PET Imaging*

SLNs were easily visualized by PET. As shown in Fig. 10, the popliteal lymph node was detected as a hot spot separated from the injection site on the coronal cross-section. This image was reconstructed from raw data acquired 15 min after injection; 0.94% of the injected dose (~0.92 pmol) accumulated in the popliteal SLN. The percent extraction was >99%. The color map represents the radioactivity counts. The SNR was 2922 for the popliteal SLN. The positioning of the hot node and the injection site was consistent to the relative locations of the fluorescence signals in optical images.

4 Discussion

A detailed optical characterization of a receptor-targeted fluorescence imaging probe is a critical step during translation into a phase 1 clinical trial. Receptor-targeted agents exhibit unique properties that offer increased sensitivity to changes in tissue function.[29] However, these properties can also limit the amount of agent that can be accumulated in the tissue. This can occur

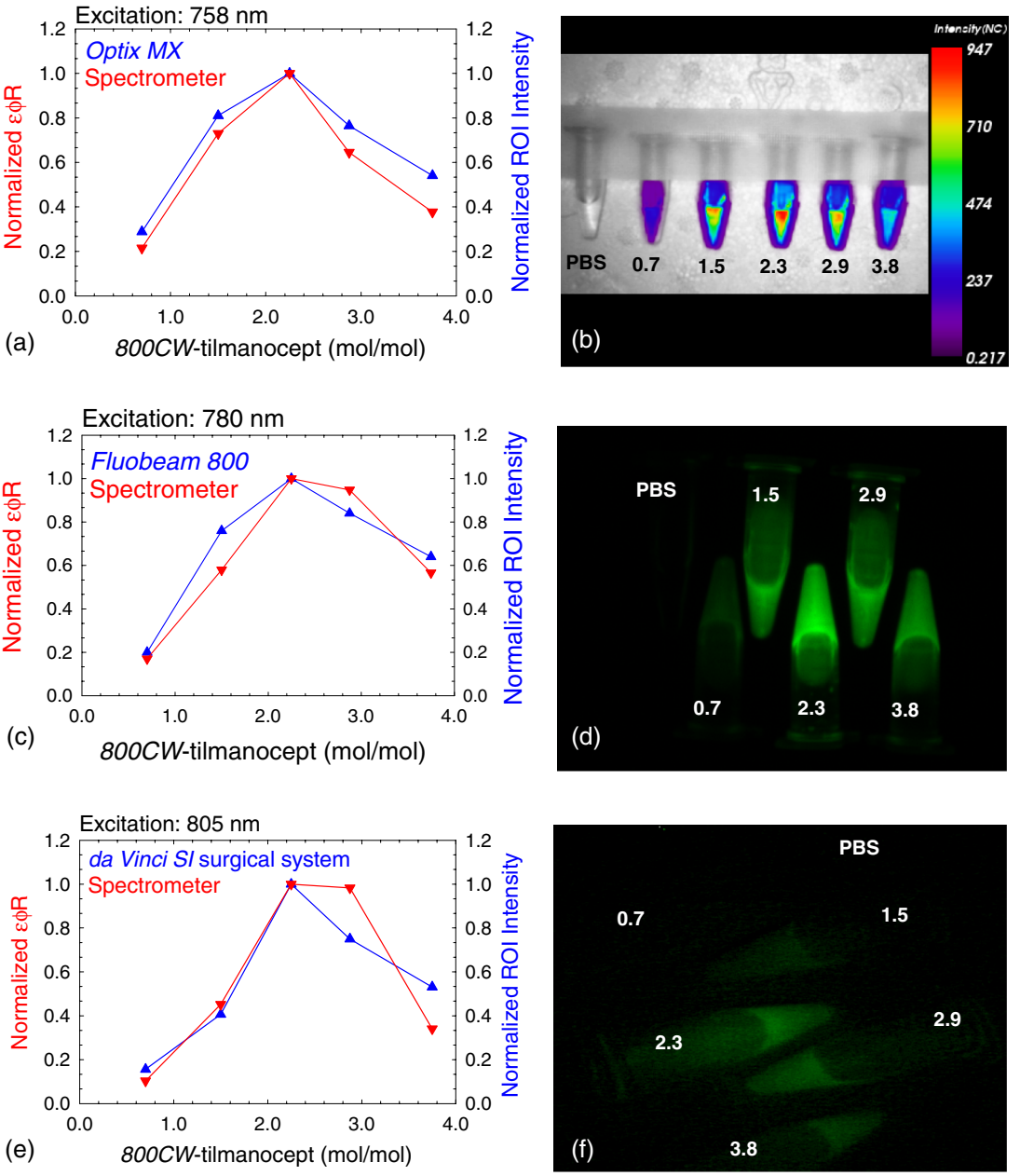

Fig. 6 The brightness calculations were confirmed by *in vitro* imaging. After normalization, the 800CW-tilmanocept (781 nM) specific fluorescence brightness $\varepsilon\Phi R$ and the ROI intensity from each fluorescence imaging system (Optix MX, Fluobeam 800, and Da Vinci SI surgical system) were compared. Normalized curves and fluorescence images at three excitation wavelengths: at 758 nm (a) and (b); at 780 nm (c) and (d); at 805 nm (e) and (f).

because the number of receptors within the target tissue will determine the maximum number of imaging molecules that can accumulate within the tissue via a receptor-targeted mechanism. Consequently, the number of imaging reporters per amount of injected probe is an important design consideration. This is the motivation for our design criteria, specific fluorescence brightness, which is an index of brightness per mole of 800CW-tilmanocept.

Specific fluorescence brightness is the optical equivalent of the specific activity for radiopharmaceuticals. The difference between the optical imaging probe and a radiopharmaceutical is that only a very small fraction of latter imaging agent is actually radiolabeled.[30] For example, when 3.0 mg of Zevalin is radiolabeled with 5.0 mCi of ^{111}In, only 0.6% of the antibodies carry a radioactive atom, the imaging reporter. Unlike radioactive labels, the attachment of more fluorescent reporters to each targeting molecule will not necessarily yield a corresponding increase in the fluorescence signal. The goal of this work was to maximize the specific fluorescence brightness of 800CW-tilmanocept.

Optimization of the IRDye 800CW loading on tilmanocept for maximum fluorescence brightness is crucial when designing the brightest conjugate. The *in vitro* brightness measurements permitted the selection of the brightest conjugate for *in vivo* studies. Fluorescence brightness trend at different wavelengths was first calculated based on absorbance and fluorescence data acquired on a spectrometer. Then this trend was further confirmed by fluorescence intensity measurements with three

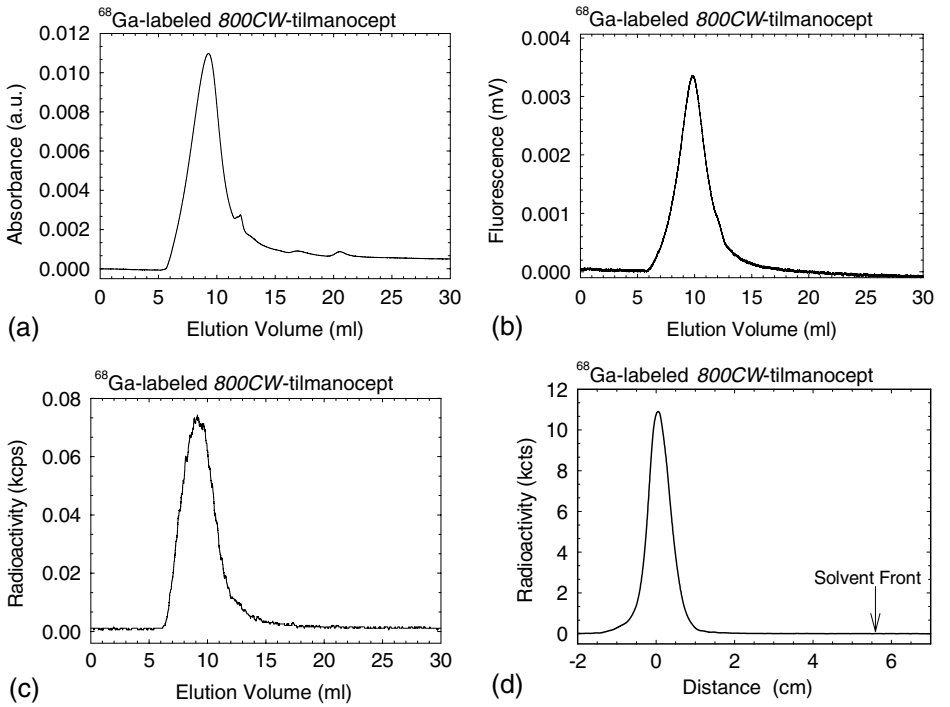

Fig. 7 Radiochemical purity of all ^{68}Ga-labeled 800CW-tilmanocept preparations. kcts = Kilocounts. High performance liquid chromatography and instant thin layer chromatography (ITLC) revealed single components within each of the (a) absorbance (226 nm), (b) fluorescence (excitation 774 nm, emission 798 nm), (c) radioactivity, and (d) ITLC radioactivity chromatograms.

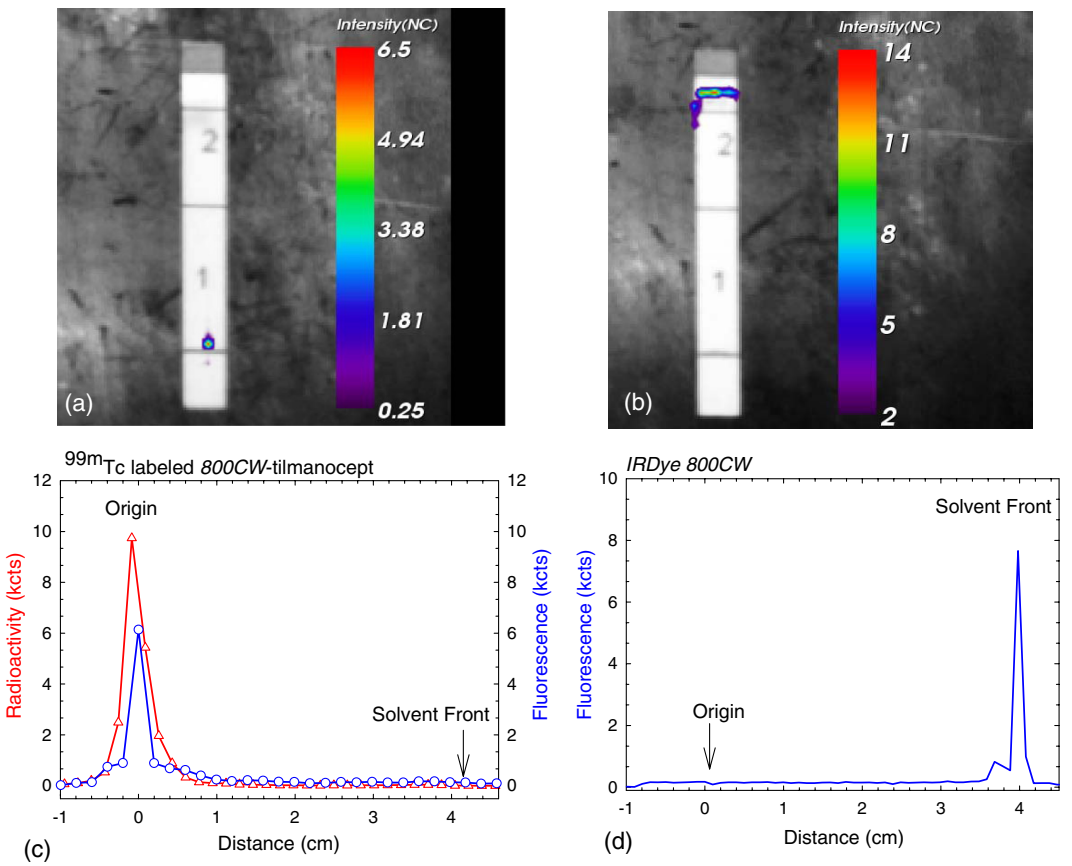

Fig. 8 Quality control of radiolabeling 800CW-tilmanocept with Ga-68. (a) Fluorescence image of a developed ITLC strip with ^{68}Ga-labeled 800CW-tilmanocept, and color map of normalized fluorescence intensity in units of counts· sec^{-1} μW^{-1}. (b) Fluorescence image of a developed ITLC strip with unconjugated IRDye 800CW. (c) Radioactivity (red, dash) and fluorescence (blue, solid) profile of an ITLC strip with ^{68}Ga-labeled 800CW-tilmanocept. (d) Fluorescence profile of an ITLC strip with unconjugated IRDye 800CW.

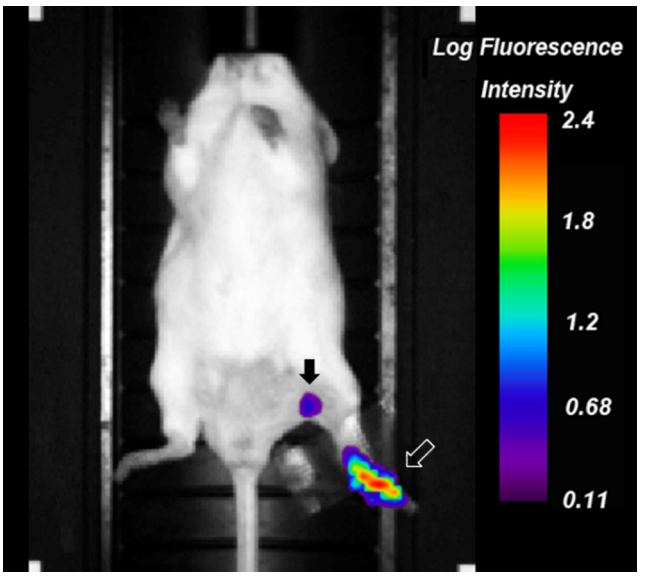

Fig. 9 A fluorescence SLN image, 25 min after the ^{68}Ga-labeled 800CW-tilmanocept ($R = 2.3$) injection into the footpad (open arrow). 1.1 pmol of 800CW-tilmanocept molecules (2.5 pmol of IRDye 800CW molecules) accumulated in the popliteal SLN (solid arrow).

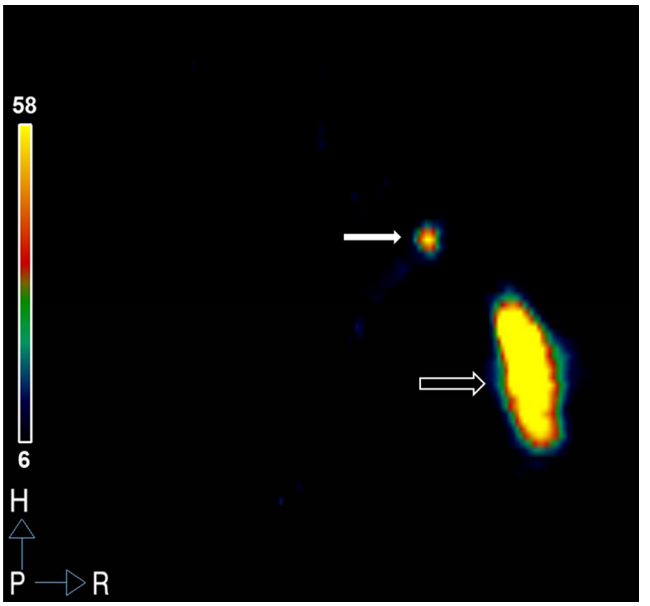

Fig. 10 A coronal PET cross-section image, 15 min after injection into the footpad (open arrow). The popliteal SLN (solid arrow) accumulated 0.92 pmol of the ^{68}Ga-labeled 800CW-tilmanocept molecules.

preclinical imaging systems. The optimal 800CW-tilmanocept conjugate peaked at the fluorophore density of $R = 2.3$. At the excitation wavelength of 758 nm, 800CW-tilmanocept with fluorophore density of $R = 2.3$ exhibited 4.7-fold stronger brightness than the conjugate with fluorophore density of $R = 3.8$. The further increase in fluorophore density does not compensate the loss of the brightness per fluorophore, which results in an overall decrement of the brightness. The trends of *in vitro* fluorescence intensity for 800CW-tilmanocept with various dye densities in PBS buffer imaged with three imaging systems match the brightness measurements on the spectrometer, where coupling 2.3 IRDye 800CW molecules per tilmanocept provides the greatest fluorescence intensity.

We evaluated the determining factors of the fluorescence brightness ($cm^{-1} \cdot mM^{-1}$), which is the product of molar absorptivity ε ($cm^{-1} \cdot mM^{-1}$), an index of how efficiently photons are absorbed, and quantum yield Φ, an index of how efficiently absorbed photons are converted to fluorescence photons. More specifically, we optimized the specific fluorescence brightness of 800CW-tilmanocept, which was an index of brightness per mole of the contrast agent. Maximum dye-loading does not necessarily yield maximum brightness. At high dye concentrations, the molar absorptivity can vary from Beer's law and the quantum yield can be reduced due to self-quenching, resulting in overall reduced brightness. Variations of absolute ε and Φ values of free IRDye 800CW were reported in literatures around 785 nm, which are possibly due to different solvent systems.[31,32]

The molar absorptivity ε per mole of dye peaked at density of $R = 2.3$. Multiple factors contribute to the changes in molar absorptivity as the number of attached dyes per dextran is increased. These factors include changes of local refractive index originating from dextran–solvent interaction,[33] dye–dye interactions,[34] and the "inner-cell" effect[35] caused by high local dye concentrations. A more detailed study into the degree at which each factor contributes to the change in molar absorptivity will require the isolation of each 800CW-tilmanocept molecule with the same degree of dye substitution. For example, a dilute solution of an 800CW-tilmanocept conjugate with only one dye attached to a single dextran may not exhibit fluorophore aggregation or an inner-cell effect.

The average Φ for unconjugated IRDye 800CW was 0.12 from direct measurement using an integration sphere. The Φ values for all the 800CW-tilmanocept conjugates fall below it and decrease with increasing fluorophore density. These could be explained by self-quenching of fluorophores in close proximity. The distribution calculations listed in Table 1 demonstrate that a fraction of the 800CW-tilmanocept molecules, even at low coupling densities, will consist of at least two IRDye 800CW moleclues attached per tilmanocept and will, consequently, facilitate self-quenching within the tilmanocept molecule, which would reduce the overall quantum yield of the molecule.

The statistical analysis sheds light on understanding the optical properties of the 800CW-tilmanocept conjugates. The essential assumption is that heavily labeled conjugates provide an increased opportunity for intramolecular interactions of the fluorophores such as inner-cell effect and self-quenching, which will consequently affect the parameters we measure, including the molar absorptivity ε and the quantum yield Φ. Our results were consistent with Gruber et al.,[36] who observed a nonfluorescent state of Cy5 at high degrees of attachment to IgG. As shown in Table 1, within the low-density 800CW-tilmanocept preparation, ~20% of the IRDye 800CW molecules contributed to 800CW-tilmanocept molecules with at least two IRDye 800CW molecules attached. This value increases to ~60% in preparations with an average of 1.0 IRDye 800CW molecule per tilmanocept. Depending on solvent and temperature, the conformation of dextran molecules changes from a rod-like shape to a random coil.[37] This conformational flexibility enables two IRDye 800CW molecules within the tilmanocept to interact and is an alternative to the hypothesis that the first dye can direct the attachment of the second dye via a dye–dye interaction.[38]

Conformational flexibility after a random attachment of the second dye would maintain the assumption of "site independence" required by the statistical model expressed by Eq. (2).

In other fluorophore-carrier systems, when switching the IRDye 800CW to other dyes such as Cy7 or Alexa 750 fluorophores, or tilmanocept to other carriers such as nanoparticles or other polymers, the optimal number of dyes per carrier may vary a great deal due to their distinct intrinsic properties (size, shape, flexibility, etc.). However, the caveat that maximum dye-loading does not equal maximum brightness is still applicable. In our case, the fluorescence intensity of the conjugate could differ by fivefold while optimizing the chemical structure. Sensitivity of the imaging system is also a limiting factor, which requires brighter probes. At same concentration, the dimmest probe may not be detectable if it is close or even beyond the detection threshold of the optical system, which could easily lead to false negatives. Furthermore, investigators need to demonstrate whether the fluorophore labeling compromises the binding affinity of the probe. Our previous study indicated fluorescent tilmanocept exhibited an unaltered K_D.[23] Similar investigations should be performed when selecting the optimal conjugate.

To the best of our knowledge, this is the first example of dual-modality nonparticulate SLN targeted imaging with ^{68}Ga and an NIR dye. Radiolabeling with ^{68}Ga greatly facilitates tracking of the 800CW-tilmanocept *in vivo* with a PET scanner. Additionally, the agent can be visualized by fluorescence and/or by a hand-held radioactivity detector. These properties make the ^{68}Ga-labeled 800CW-tilmanocept ideal for preoperative surgical planning. Hybrid PET-CT can guide the surgeon to the lymph node basin that contains the SLN. Fluorescence imaging cameras such as the Fluobeam[38] can guide the surgical exposure and visual identification of the SLN.[39] This can be performed with wide-bandwidth cameras and laparoscopic cameras during robotic-assisted surgery.[40] The goal of the approach is to reduce operative time, improve diagnostic accuracy, and decrease morbidity.

Acknowledgments

We thank Professor Roger Y. Tsien for the use of his Fluorolog spectrometer and his trenchant observations during our many discussions. We appreciate the thoughtful discussions with Dr. Dan Draney and kind reviews from Ms. Joy Kovar and Dr. Brad Roth at LI-COR Biosciences. IRDye 800CW was a generous gift from LI-COR Biosciences. We acknowledge Horiba Scientific Inc. for the absolute quantum yield measurement of the free unconjugated IRDye 800CW. This research was supported by the National Institutes of Health (Grants P50 CA128346 and P30 CA023100).

References

1. R. M. Cabanas, "An approach for the treatment of penile carcinoma," *Cancer* **39**(2), 491–499 (1977).
2. D. L. Morton et al., "Technical details of intraoperative lymphatic mapping for early stage melanoma," *Arch. Surg.* **127**(4), 392–399 (1992).
3. J. C. Alex and D. N. Krag, "Gamma-probe guided localization of lymph nodes," *Surg. Oncol.* **2**(3), 137–143 (1993).
4. J. J. Albertini et al., "Intraoperative radiolymphoscintigraphy improves sentinel lymph node identification for patients with melanoma," *Ann. Surg.* **223**(2), 217–224 (1996).
5. M. B. Faries and D. L. Morton, "Surgery and sentinel lymph node biopsy," *Semin. Oncol.* **34**(6), 498–508 (2007).
6. D. L. Morton et al. "Sentinel node biopsy for early-stage melanoma: accuracy and morbidity in MSLT-I, an international multicenter trial," *Ann. Surg.* **242**(3), 302–311; discussion 311–303 (2005).
7. K. T. Cheng et al., "^{99m}Tc-diethylenetriaminepentaacetic acid-mannosyl-dextran," in *Molecular Imaging and Contrast Agent Database*, National Center for Biotechnology Information, Bethesda, MD (2011).
8. D. R. Vera et al., "A synthetic macromolecule for sentinel node detection: [^{99m}Tc]DTPA-mannosyl-dextran," *J. Nucl. Med.* **42**(6), 951–959 (2001).
9. D. R. Vera et al., "[^{99m}Tc]tilmanocept: a synthetic receptor-targeted molecule for sentinel lymph node mapping," in *Radiopharmaceuticals for Sentinel Lymph Node Detection*, International Atomic Energy Agency, Vienna (in press).
10. A. M. Wallace et al., "Lymphoseek: a molecular imaging agent for melanoma sentinel lymph node mapping," *Ann. Surg. Oncol.* **14**(2), 913–921 (2007).
11. A. M. Wallace et al., "Lymphoseek: a molecular radiopharmceutical for sentinel node detection," *Ann. Surg. Oncol.* **10**(5), 531–538 (2003).
12. S. P. L. Leong et al., "A phase 2 study of [^{99m}Tc]tilmanocept in the detection of sentinel lymph nodes in melanoma and breast cancer," *Ann. Surg. Oncol.* **18**(4), 961–969 (2011).
13. V. K. Sondak et al., "Combined analysis of phase III trials evaluating [^{99m}Tc]tilmanocept and vital blue dye for identification of sentinel lymph nodes in clinically node-negative cutaneous melanoma," *Ann. Surg. Oncol.* **20**(2), 680–688 (2013).
14. A. M. Wallace et al., "Comparative evaluation of [^{99m}Tc]tilmanocept for sentinel lymph node mapping in breast cancer patients: result of two phase 3 trials," *Ann. Surg. Oncol.* **20**(8), 2590–2599 (2013).
15. "^{99m}Tc-tilmanocept approval," *J. Nucl. Med.* **54**(5), 20N (2013).
16. H. G. van der Poel et al., "Intraoperative laparoscopic fluorescence guidance to the sentinel lymph node in prostate cancer patients: clinical proof of concept of an integrated functional imaging approach using a multimodel tracer," *Eur. Urol.* **60**(4), 826–833 (2011).
17. O. R. Brouwer et al., "Comparing the hybrid fluorescent-radioactive tracer indocyanine green-^{99m}Tc-nanocolloid with ^{99m}Tc-nanocolloid for sentinel node identification: a validation study using lymphoscintigraphy and SPECT/CT," *J. Nucl. Med.* **53**(7), 1034–1040 (2012).
18. I. J. Fox et al., "A tricarbocyanine dye for continuous recording of dilution curves in whole blood independent of variations in blood oxygen saturation," *Proc. Staff Meet. Mayo Clin.* **32**(18), 478–484 (1957).
19. *Summary of Product Characteristics for Nanocoll, Kit for Radiopharmaceutical Preparation*, GE Healthcare S.R.L., Milan, Italy (2009).
20. S. E. Strand and B. R. R. Persson, "Quantitative lymphoscintigraphy I: Basic concepts for optimal uptake of radiocolloids in the parasternal lymph nodes of rabbits," *J. Nucl. Med.* **20**(10), 1038–1046 (1979).
21. S. P. Stroup et al., "Preoperative sentinel lymph node mapping of the prostate using PET/CT fusion imaging and Ga-68-labeled tilmanocept in a dog model," *Clin. Exp. Metastasis* **29**(7), 673–680 (2012).
22. R. Ting et al., "Fast F-18 labeling of a near-infrared fluorophore enables positron emission tomography and optical imaging of sentinel lymph nodes," *Bioconjug. Chem.* **21**(10), 1811–1819 (2010).
23. D. K. Emerson et al., "A receptor-targeted fluorescent radiopharmaceutical for multireporter sentinel lymph node imaging," *Radiology* **265**(1), 186–193 (2012).
24. D. R. Vera et al., "Cy5.5-DTPA-galactosyl-dextran: a fluorescent probe for in vivo measurement of receptor biochemistry," *Nucl. Med. Biol.* **32**(7), 687–693 (2005).
25. J. L. Oncley, "Interpretation of data obtained in studies with isotope-labeled proteins of biological significance; chemical considerations," *Fed. Proc.* **16**(suppl 2), 3–6 (1957).
26. C. F. Meares and D. A. Goodwin, "Linking radiometals to proteins with bifunctional chelating agents," *J. Protein Chem.* **3**(2), 215–228 (1984).
27. A. T. R. Williams, S. A. Winfield, and J. N. Miller, "Relative fluorescence quantum yields using a computer-controlled luminescence spectrometer," *Analyst* **108**(1290), 1067–1071 (1983).
28. P. R. Bevington, "Propagation of errors," in *Data Reduction and Error Analysis for the Physical Sciences*, pp. 56–65, McGraw-Hill, Dubuque, Iowa (2003).
29. D. R. Vera, E. S. Woodle, and R. C. Stadalnik, "Kinetic sensitivity of a receptor-binding radiopharmaceutical: technetium-99m-galactosyl-neoglycoalbumin," *J. Nucl. Med.* **30**(9), 1519–1530 (1989).

30. W. C. Eckelman, M. Bonardi, and W. A. Volkert, "True radiotracers: are we approaching theoretical specific activity with Tc-99m and I-123?," *Nucl. Med. Biol.* **35**(5), 523–527 (2008).
31. A. Azhdarinia et al., "Characterization of chemical, radiochemical and optical properties of a dual-labeled MMP-9 targeting peptide," *Bioorgan. Med. Chem.* **19**(12), 3769–3776 (2011).
32. H. S. Choi et al., "Synthesis and in vivo fate of zwitterionic near-infrared fluorophores," *Angew. Chem. Int. Edit.* **50**(28), 6258–6263 (2011).
33. D. Toptygin, "Effects of the solvent refractive index and its dispersion on the radioactive decay rate and extinction coefficient of a fluorescent solute," *J. Fluoresc.* **13**(3), 201–219 (2003).
34. A. Mishra et al., "Cyanines during the 1990s: a review," *Chem. Rev.* **100**(6), 1973–2011 (2000).
35. G. G. Guilbalt, "General aspects of luminescence spectroscopy," in *Practical Fluorescence*, pp. 30–32, Marcel Dekker Inc., New York (1990).
36. H. J. Gruber et al., "Anomalous fluorescence enhancement of Cy3 and Cy3.5 versus anomalous fluorescence loss of Cy5 and Cy7 upon covalent linking to IgG and noncovalent binding to avidin," *Bioconjug. Chem.* **11**(5), 696–704 (2000).
37. A. M. Basedow and K. H. Ebert, "Production, characterization, and solution properties of dextran fractions of narrow molecualar weight distributions," *J. Polym. Sci. Pol. Sym.* **66**(1), 101–115 (1979).
38. M. Keramidas et al., "Intraoperative near-infrared image-guided surgery for peritoneal carcinomatosis in a preclinical experimental model," *Br. J. Surg.* **97**(5), 737–743 (2010).
39. Y. Kawaguchi et al., "Hepatobiliary surgery guided by a novel fluorescent imaging technique for visualizing hepatic arteries, bile ducts, and liver cancers on color images," *J. Am. Coll. Surgeons* **212**(6), E33–E39 (2011).
40. B. N. Breyer et al., "Pelvic lymphadenectomy in prostate cancer," *Prostate Cancer P. D.* **11**(4), 320–324 (2008).